Effect of relative humidity on contact angle and particle deposition morphology of an evaporating colloidal drop

Viral H. Chhasatia, Abhijit S. Joshi, and Ying Sun[a)]
Drexel University, Philadelphia, Pennsylvania 19104, USA

(Received 19 October 2010; accepted 16 November 2010; published online 10 December 2010)

The deposition behavior of inkjet-printed aqueous colloidal drops on a glass substrate has been investigated by using fluorescence microscopy and a high resolution goniometer. Real-time side-view images of a pinned colloidal drop show that the contact angle during evaporation is a function of the relative humidity (RH). The RH also affects the extent to which the drop is able to spread after impacting a substrate, the evaporation rate at the drop surface, and the evaporatively driven flow inside the drop that drives the suspended particles toward the contact line. Results show that the particle deposition area and pattern change significantly with the RH. © *2010 American Institute of Physics*. [doi:10.1063/1.3525167]

An evaporating colloidal drop usually leaves the residual particles in a coffee-ring pattern along the original wet surface boundary due to higher evaporation rates near the droplet contact line, as explained by Deegan *et al.*[1] Surface tension driven Marangoni flow induced due to temperature[2] and concentration (using solvent mixture)[3] gradients can enhance or suppress the particle motion toward the contact line, thereby modifying the coffee-ring deposition. Picoliter aqueous colloidal drops used in inkjet printing evaporate within seconds, leaving evaporative and Marangoni flows as the dominant factors affecting particle deposition. The relative humidity (RH) of the ambient air is one of the several factors that affect the evaporation rate. Besides the fact that RH directly influences the drop evaporation rate, i.e., a drop evaporates faster at lower RH values, Anderson and Davis[4] demonstrated that evaporation rate affects the spreading behavior of a liquid drop. Their analysis showed that the increase in dynamic contact angle during drop spreading is a result of the difference between the liquid velocity near the contact line and the contact line velocity, induced by drop evaporation. Similarly, evaporation rate affecting the spreading of liquid films has been demonstrated by Ajaev *et al.*,[5] where the evaporation rate is modified by heating the substrate.

However, the effect of evaporation rate on colloidal drop spreading and subsequent particle deposition has not been examined in detail, although this process is at the core of emerging technologies such as inkjet-printing-based additive manufacturing of functional materials into printable electronics and photovoltaics.[6–8] In this letter, we present experimental results for inkjet-printed, evaporating picoliter aqueous colloidal drops, where the mass loss due to evaporation is significant. The drop evaporation rate is modified by changing the RH inside an environmental chamber. A colloidal mixture of carboxylate-modified polystyrene fluorescent beads of 1.1 μm diameter in de-ionized water, 0.5% by volume, is used. Picoliter drops are generated using a piezoelectric-driven inkjetting nozzle (MicroFab MJ-AL01-60, Plano, Texas). A high resolution (0.5 μm/pixel) charge-coupled device (CCD) camera system, consisting of a SensiCam QE CCD camera (Romulus, Michigan) and a Navitar 12× Zoom lens (Rochester, New York), is synchronized with a halogen strobe light and the drop ejection to form a high magnification goniometer for side-view observation of drop evaporation.

Particle motion and deposition inside the colloidal drop are observed using a Zeiss inverted fluorescence microscope (Thornwood, New York) with a 20× objective and bottom-view images are captured by a Sony XCL-5005CR CCD camera (Park Ridge, New Jersey). The bottom-view and side-view cameras are both capable of capturing more than 10 frames/second. The RH levels inside the environmental chamber are controlled by supplying either dry or humid air, and RH levels of 10%, 30%, and 60% are obtained during the experiments. The ambient temperature is kept at 22 °C for all experiments. Details of the experimental setup are described elsewhere.[9] Contact angle measurements for side-view images have been carried out using IMAGEJ (http://rsbweb.nih.gov/ij/) assuming that the drop interface remains a spherical cap at all times. Neglecting gravitational distortion of the drop surface is justified because the Bond number is less than 0.005.

Figure 1 shows the evaporation dynamics of an inkjet-printed aqueous colloidal drop on a glass substrate. The base radius of the drop is denoted by R_b and the radius of the spherical cap is R. Upon impact, the inkjet-printed colloidal drop spreads to its maximum radius on a glass substrate within the first 0.1 s. The drop contact line is then pinned at this maximum radius, due to chemical heterogeneity or nanoscale roughness of the substrate, and remains pinned during the entire drop evaporation process, as shown in both sides [Fig. 1(a)] and bottom view [Fig. 1(b)]. The decrease in the drop height and contact angle θ is observed in the side-view images as time progresses. Bottom-view images [Fig. 1(b)] show the evaporatively driven motion of individual 1.1 μm particles toward the pinned contact line. These particles further enhance contact line pinning. It is observed that the contact angle reduces to almost 0° during the final stages of evaporation. However, as shown in Fig. 1(c), the water film starts to recede near the end of the evaporation as significant mass loss due to evaporation, which makes the maintenance

[a)]Author to whom correspondence should be addressed. Department of Mechanical Engineering and Mechanics, Drexel University, Philadelphia, PA 19104. Tel.: +1(215)895-1373. FAX: +1(215)895-1478. Electronic mail: ysun@coe.drexel.edu.

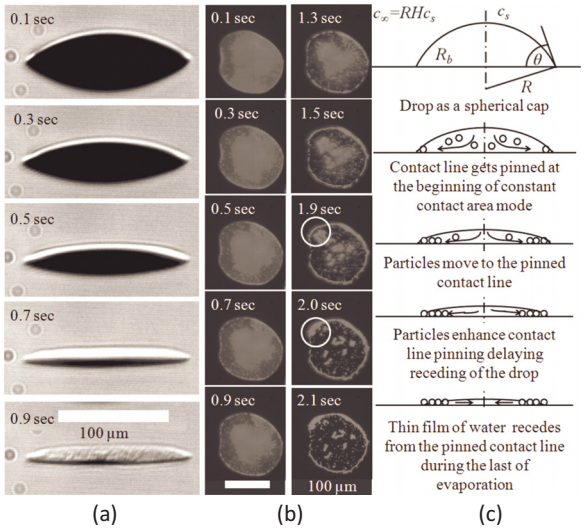

FIG. 1. (Color online) Snapshots of a drying colloidal drop at 60% relative humidity on a glass substrate from (a) side view, (b) bottom view, and (c) schematic of the pinned evaporation process. Particle movement toward the pinned contact line can be observed clearly between 1.9 and 2 s (circled areas).

of the film unsustainable, leaving colloidal particles to form a coffee-ring deposit on the substrate. Film evaporation can only be observed in the bottom view because once the contact angle (θ) of the drop falls below 5°, side-view images appear similar from 0.9 to 2.1 s.

One of the central themes we want to explore in this letter is the effect of evaporation rate on the contact angle. Empirical studies of the spreading of nonvolatile liquids on solid surfaces have led to a constitutive relation between the instantaneous (dynamic) advancing contact angle θ_A and the fluid velocity parallel to the substrate (U_{CL}), which is given by[4]

$$U_{\mathrm{CL}} = \eta(\theta_A - \theta_{A,\mathrm{static}})^m, \tag{1}$$

where $\theta_{A,\mathrm{static}}$ is the static advancing contact angle, and η and m are the empirically determined constants. In the absence of evaporation, the contact line velocity dR_b/dt is equal to U_{CL}, satisfying mass conservation. However, if there is an evaporative mass loss J, the appropriate form of mass conservation is now given by[4]

$$\frac{dR_b}{dt} = U_{\mathrm{CL}} - \frac{J}{\rho_l \sin(\tilde{\theta}_A)}, \tag{2}$$

where $\tilde{\theta}_A$ is the (instantaneous) advancing contact angle in the presence of evaporation. Recent experiments for volatile liquids[5] have revealed that $\tilde{\theta}_{A,\mathrm{static}} > \theta_{A,\mathrm{static}}$ and $\tilde{\theta}_A > \theta_A$. Following Ref. 4, we assume that an expression similar to Eq. (1) is applicable even for volatile drops, which implies that

$$U_{\mathrm{CL}} = \eta(\tilde{\theta}_A - \tilde{\theta}_{A,\mathrm{static}})^m. \tag{3}$$

While the exact validity of Eq. (3) is not yet known, our conclusions will not be affected as long as U_{CL} increases with $\tilde{\theta}_A - \tilde{\theta}_{A,\mathrm{static}}$.

At the precise instant in time when the contact line reaches its maximum radius and gets pinned, $dR_b/dt = 0$ and Eq. (3) can be combined with Eq. (2) to obtain $\rho_l \sin(\tilde{\theta}_A)\eta(\tilde{\theta}_A - \tilde{\theta}_{A,\mathrm{static}})^m = J$. Thus, $J > 0$ implies that $\tilde{\theta}_A - \tilde{\theta}_{A,\mathrm{static}} > 0$.

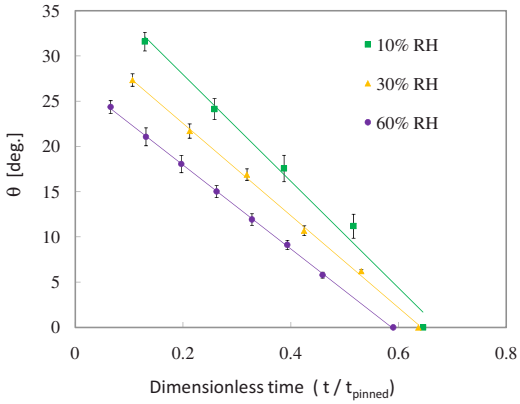

FIG. 2. (Color online) Contact angle of the drop as a function of nondimensional time at different RH values.

Equation (3) implies that $\tilde{\theta}_A - \tilde{\theta}_{A,\mathrm{static}} > 0$ during the initial spreading process (moving contact line). However, the above analysis shows that when $J > 0$, $\tilde{\theta}_A - \tilde{\theta}_{A,\mathrm{static}} > 0$ even when the contact line has reached its maximum radius and has stopped moving. Although $\tilde{\theta}_{A,\mathrm{static}}$ increases with J,[5] it can be argued that the difference $\tilde{\theta}_A - \tilde{\theta}_{A,\mathrm{static}}$ remains approximately constant and does not vary significantly with J. In this case, the measured contact angle $\tilde{\theta}_A$ clearly increases with J because $\sin(\tilde{\theta}_A)$ is proportional to J.

Figure 2 plots the experimentally measured contact angle θ as a function of time for various RH values. It can be observed that the initial value of θ (when the contact line pins) is larger for higher evaporation rates (larger J, lower RH), confirming our theoretical analysis. The angle θ subsequently reduces for each RH value because of continued contact line pinning and evaporation. Note that the above theoretical analysis is valid only until the contact line first pins and the subsequent reduction of θ with time, as shown in Fig. 2, is dependent solely on the evaporation rate. For each RH value, contact angle measurements are carried out until the side-view images no longer change with time, typically until $\theta < 5°$. As discussed before (Fig. 1), we recognize that the evaporation process is not complete at this point, but measurement of contact angles (using the side-view camera) is no longer meaningful beyond this point. Therefore, reported values of the evaporation time for experiments correspond to these side-view observations. Each data point in Fig. 2 is the average contact angle for five different drops at different locations on the substrate and error bars represent the standard deviation.

To gain more insight into the evaporation process, the experimental time for each RH value in Fig. 2 has been scaled by the theoretical evaporation time for that RH value for a pure water drop. Birdi *et al.*[10] expressed the rate of evaporation as $\rho_l(dV/dt) = -4\pi R^2 D(dC/dr)$ in the quasisteady-state diffusion-driven evaporation of a spherical water drop of radius R, where V is the volume of the drop, D is the diffusion coefficient of water vapor in the air, and C is the water vapor concentration in air. It is assumed that $C = C_s$ (saturated concentration) at the drop surface and $C = C_\infty$ far away from the drop surface. With these boundary conditions, the evaporation rate can be expressed as

$$\rho_l \frac{dV}{dt} = -4\pi DR(C_s - C_\infty)F(\theta), \tag{4}$$

where $F(\theta)$ is a function introduced by Picknett and Bexon[11] to accommodate the effect of a solid surface on the vapor field. By making an analogy to an electrostatics problem of evaluating the capacitance of a conductor of the same shape as the sessile drop, an exact solution for $F(\theta)$ was obtained.[11]

The volume of a spherical cap with base radius R_b and contact angle θ [see Fig. 1(c)] is given by $V=\frac{1}{3}\pi R_b^3\beta(\theta)$, where $\beta(\theta)=[2-3\cos(\theta)+\cos^3(\theta)]/\sin^3(\theta)$. Using this relationship and defining $\mathrm{RH}=C_\infty/C_s$, Eq. (4) can be written as

$$\frac{\pi R_b^2}{3}\frac{d}{dt}\beta(\theta) = \frac{-4\pi DC_s(1-\mathrm{RH})}{\rho_l \sin(\theta)}F(\theta). \tag{5}$$

Further rearrangement of Eq. (5) leads to

$$\frac{d\theta}{dt} = \frac{-4DC_s(1-\mathrm{RH})}{\rho_l R_b^2}\frac{2+\cos\theta}{\beta(\theta)}F(\theta). \tag{6}$$

Equation (6) may be integrated to solve for the time interval the drop spends in the pinned stage of the evaporation (t_{pinned}), which is thus given by

$$t_{\mathrm{pinned}} = \frac{\rho_l R_b^2}{4DC_s(1-\mathrm{RH})}\int_0^\theta \frac{\beta(\theta)}{(2+\cos\theta)F(\theta)}d\theta. \tag{7}$$

For a fixed value of RH, the contact angle decreases linearly with time, as shown in Fig. 2, which is consistent with the observations in literature[10] for a fixed evaporation rate. Theoretical values of t_{pinned} using Eq. (7) for 10%, 30%, and 60% RH are 0.8, 0.9, and 1.5 s, respectively. The actual evaporation times in our experiments are 0.5, 0.6, and 0.9 s, respectively. These discrepancies are thought to arise because of two reasons: (i) the presence of suspended particles in experiments, which is not accounted for while deriving Eq. (7) above, and (ii) the evaporation time reported for our experiments corresponds to observations from the side-view camera and does not include the time spent in the final stages of evaporation, which is more akin to film evaporation, as discussed earlier with reference to Fig. 1(c).

Finally, we observe that the particle deposit area A, which is the area bounded by the outer edge of the coffee ring, decreases as the RH increases. To quantify this increase in area, we calculate the deposition diameter (d) by measuring the contact area A using IMAGEJ and using the relation $A=\pi d^2/4$ to calculate the diameter. The bottom-view images of the particle deposits and the deposit diameters for different RH values are shown in Fig. 3. At 10% RH, the final particle deposition diameter is 120 μm, and this diameter increases with increasing RH. Each data point in Fig. 3 is the average of ten diameter measurements for ten different deposits at different locations on the substrate, and error bars represent the standard deviation. Because the contact line does not recede during evaporation, deposition diameter changes very little during the final stages of the evaporation resulting in deposition area similar to the initial drop spreading area. The observed higher deposition diameter at higher RH (low evaporation rate) can be attributed to a lower contact angle during spreading, as discussed before and shown in Fig. 2. It can also be observed from Fig. 3 that the circularity of the final deposit deteriorates with increasing RH. This is probably caused by an enhancement of the effect of local nonuniformities on the glass substrate at lower contact angles.

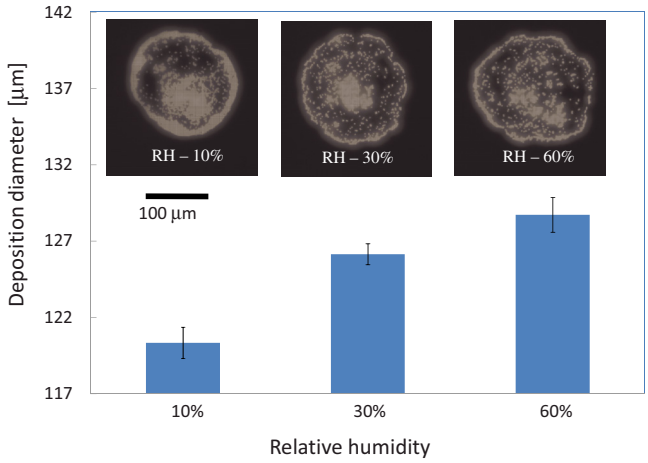

FIG. 3. (Color online) Final deposition morphology as a function of the RH. The scale bar (100 μm) is the same for all images.

In conclusion, because of the small (picoliter) volume of the drops in inkjet printing, the RH becomes a dominant process parameter, dictating evaporation rates and deposition dynamics of aqueous colloidal drops. It is found that as the RH increases, slower evaporation results in lower contact angle of the drop and more spreading. More spreading of the drop leads to a larger particle deposition area for a pinned drop. Thus, controlling the RH is critical in ensuring repeatability of deposited patterns in inkjet printing.

Support for this work was provided by the National Science Foundation (Grant No. CAREER-0968927). The authors would also like to thank Ahmad Hijazi, Richard Vallett, and Angela Miller for measuring contact angles of the evaporating colloidal drops.

[1] R. D. Deegan, O. Bakajin, T. F. Dupant, G. Huber, S. R. Nagel, and T. A. Witten, Nature (London) **389**, 827 (1997).
[2] H. Hu and R. G. Larson, J. Phys. Chem. B **110**, 7090 (2006).
[3] J. Park and J. Moon, Langmuir **22**, 3506 (2006).
[4] D. M. Anderson and S. H. Davis, Phys. Fluids **7**, 248 (1995).
[5] V. S. Ajaev, T. Gambaryan-Roisman, and P. Stephan, J. Colloid Interface Sci. **342**, 550 (2010).
[6] E. Tekin, P. J. Smith, and U. S. Schubert, Soft Matter **4**, 703 (2008).
[7] H. A. Haverinen, R. A. Myllylä, and G. E. Jabbour, Appl. Phys. Lett. **94**, 073108 (2009).
[8] M. Walther, A. Ortner, H. Meier, U. Löffelmann, P. J. Smith, and J. G. Korvink, Appl. Phys. Lett. **95**, 251107 (2009).
[9] S. Biswas, S. Gawande, V. Bromberg, and Y. Sun, ASME J. Sol. Energy Eng. **132**, 021010 (2010).
[10] K. S. Birdi, D. T. Vu, and A. Winter, J. Phys. Chem. **93**, 3702 (1989).
[11] R. G. Picknett and R. Bexon, J. Colloid Interface Sci. **61**, 336 (1977).